ADRIS: an Automatic Diabetic Retinal Image Screening system

Kheng Guan GOH, Wynne HSU, Mong Li LEE, Huan WANG
School of Computing
National University of Singapore
Singapore 119260
{gohkg, whsu, leeml, wangh}@comp.nus.edu.sg

Diabetic-related eye disease is the most common cause of blindness worldwide. The most effective treatment is early detection through regular screenings. This produces a large number of retinal photographs for the medical doctors to review. In our work, we employ a combination of innovative image processing and data mining techniques to automate the preliminary analysis and diagnosis of diabetic-related eye disease from the digitised retinal photographs. Our experimental results show that we are able to accurately detect abnormal symptomssuch as: abnormal optic disc to cup ratio, presence of exudates and tortuous blood vessels. With this, our system is able to classify the retinal images into normal and abnormal ones, thus cutting down on the number of retinal photographs a doctor needs to review.

1   Introduction

More than half (57.6%) of all newly registered blindness in Singapore is caused by retinal diseases, as reported by Lim (1999). Diabetic retinopathy (19.4%) is one of the main contributors. As Singapore has one of the fastest ageing population in the world and about 10% of Singaporeans are diabetic, as reported by Goh (1998), diabetic-related eye diseases are set to rise. Industrialised countries in the world are facing the same problem. For example, in the United States blindness has been estimated to be 25 times more common in people with diabetes than in those without the disease (Kahn and Hiller, 1974; Palmberg, 1977), and yearly 5000 new cases of blindness are reported as a result of diabetic retinopathy (Klein *et al.*, 1995; Javitt et al., 1989) In the United Kingdom, diabetic eye diseases are the most common cause of blindness in the country for the age group of 20 to 65 (Ghafour *et al.*, 1983).

The most effective treatment to combat these eye diseases is early detection through regular screening of the fundus to detect early signs of diabetic retinopathy, as reported by Singer *et al.* (Singer *et al.*, 1992). Early detection screenings consist primarily of obtaining fundus images through photography. However, with a large number of patients undergoing regular screenings, tremendous amount of time is needed for the medical professionals to analyse and diagnose the fundus photographs. As a result, this may delay the patients from being referred to ophthalmologist for further examination and treatment. Therefore, by automating the initial task of analysing the huge amount of retinal photographs for symptoms of diabetic retinopathy, the efficiency of the screening process can be greatly improved. At the same time, patients that require the attention of the ophthalmologist would be timely referred.

We have developed an Automatic Diabetic Retinal Image Screening system (ADRIS), which combines novel image processing techniques with data mining technique to analyse digitised diabetic retinal photographs. Based on the rules given by medical experts, the system classifies the retinal images into normal (healthy) and abnormal (unhealthy) ones. Once a diabetic retinal image is found to have any abnormal feature, the system would highlight it to the doctor for review. Initial studies indicate that the system can potentially reduce the number of retinal photos a doctor needs to review by more than 60%.

2   Understanding the Problem Domain

It has been estimated that to implement a regular screening programme for diabetic patients, 30,000 patients per million total populations would be involved (Retinopathy Working Party, 1991). Hence over the years, there have been quite a number of developments in automatic screening and detection of diabetic retinopathy and other age-related diseases. Gardner *et al.* (1996) concluded in their studies that a neural network program could be trained to detect retinal images with diabetic retinopathy features. Numerous systems (Ward *et al.*, 1989; Spencer *et al.*, 1992; Spencer *et al.*, 1991; Katz *et al.*, 1988; Katz *et al.*, 1990) reported some successes in the automatic detection of glaucoma, exudates, microaneurysm and maculopathy in diabetic retinopathy. However, an application in automatic diabetic retinal screening has yet to be developed and implemented.

Cox *et al.* (1991) used grey level information around the vicinity to automatically extract the boundary of the optic disc with initial approximate location given by the user input. Morris *et al.* (1994) employed dynamic contour to map out the boundary of the optic disc. Their approach is

dependent on image pre-possessing where there is a heavy emphasis on enhancing the image contrast.

Phillips *et al.* (1993) used simple thresholding method to detect and quantify exudates. Global and local thresholding levels are used for extracting large and small exudate respectively. However, their straightforward approach generated some false-negatives due to the presence of exudates with low grey level intensity. Leistritz *et al.* (1994) acquired retinal images through scanning laser ophthalmoscope with monochromatic illumination to detect exudates with the highest contrast. However, images have to be captured with a suitable wavelength for this approach to be reliable.

Zhou *et al.* (1994) used match-filtering approach with *priori* knowledge to automatically extract and track retinal vessel in digital fluorescein angiograms. Zana *et al.* (1997) used mathematical morphology and linear processing techniques that include Laplacian filter and curvature differentiation to extract retinal blood vessel in retinal angiography. Both approaches are targeted at retinal angiograms. Capowski *et al.* (1993) employed *relative length variation* (arc/chord information) to ascertain the tortuousity of retinal blood vessel manually.

2.1   Data Mining Applications On Medical data

The prevalence of large databases created a need to devise new tools that can sift out useful and interesting knowledge from these data. As a result, a new research area, data mining and knowledge discovery is rapidly gaining popularity.

Data mining is the application of specific algorithms for extracting interesting patterns from data, (Fayyad *et al.*, 1996). Large databases contain vast amount of data which is most often left hidden from the user. These hidden data might harbour some very useful relationships (e.g. in the diabetic retinal screening database patients of certain race with a minimum number of years of illness might have a certain percentage of likelihood that eye disease may develop within a certain number of years), trends (e.g. the deterioration of a particular eye disease might localise around a certain race or gender based on patient's lifestyle and age of employment) and prediction (e.g. based on past data, a prediction of certain accuracy can be made on whether a new patient is going to develop diabetic-related eye disease), etc.

Classification-Based on Association (CBA, Liu *et al.*, 1998) is a data mining tool that combines classification rule mining and association rule mining to take advantage of the benefits of both methods. Classification

rule mining separates the data into different classes based on a small set of rules in the database. And the target of classification rule mining is pre-determined. In association rule mining, constraints such as minimum confidence and minimum support are used to discover all the rules in the database. And the targets in association rule mining are not pre-determined.

Some of the research and applications carried out using knowledge discovery techniques in medical domains (notably medical diagnosis) includes oncology, Elomaa and Holsti (1989); liver pathology, Lesmo *et al.* (1984); urology, Bratko and Kononenko (1987) ; thyroid disease diagnosis, Hojker *et al.* (1988); rheumatology, Kern *et al.* (1990); neuropsychology, Muggleton (1990); abdominal pain diagnosis, Provan *et al.* (1996) and gynaecology, Nunez (1990).

In our system, we use an association based data mining classification tool developed by Liu *et al.* (1998) to discover the association rules between the different curvature definitions of retinal blood vessels.

3   Understanding the Data

Figure 1 shows a healthy normal fundus image which has the following features:

I. Optic disc

Colour:	Red-yellow; the yellowish colour (optic cup) is more pronounced on the temporal and the nasal side part may appear pale.
Form and size:	Round to oval with diameter ranging from 1.5mm to 1.7mm.
Margins:	Sharply outline.
Vessels:	They originate within the perimeter of the disc and both the arteries and veins appear distinct.

II. Vessels

Colour:	Arteries appear light red while veins appear dark red.
Form and size:	Largely straight with gentle curves. The arteries appear somewhat narrower than the veins, with an average ratio of 2:3 between arteries and veins. Average diameter of veins is 125μm.
Margins:	Generally more sharply outline in the centre than at the peripheral.

III. Macular

Colour: Appears darker than the surrounding retina.

Form and size: Lies in the optic axis of the eye and is situated about 2 disc (3 ~ 4 mm) diameter temporal from the optic disc.

Margins: Not clearly defined in normal illumination. Marginally visible in red free illumination.

IV. Choroid

Colour: Reddish colour.

Margins: Normal even appearance throughout the inter-vascular space.

Figure 1. Sample of a healthy normal fundus image

On the other hand, a diabetic retinopathy fundus will exhibit some of the following symptoms as shown in Figure 2:

i. Abnormal Optic Disc and Cup ratio

The centre of the optic disc has a small white depression, optic cup (physiologic excavation). Under normal healthy circumstances, the size of the optic cup is about 40% or less compared to the optic disc. Abnormal condition appears when the optic disc is not visible, the outline is not circular, or it appears completely white (only the optic cup is visible).

ii. Presence of Exudates

Exudates show up as random white patches around the inter-vascular region. They vary in shapes and sizes.

iii. Tortuous Vessels

Normal retinal blood vessels appear largely straight or gently curved. In some diseases, the blood vessels become tortuous, i.e. they become dilated and take on a wavy path.
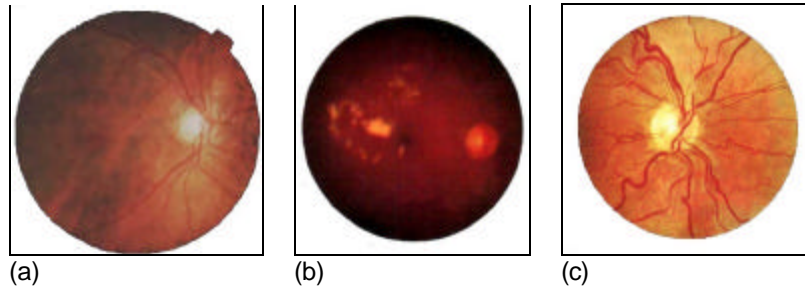
(a)   (b)   (c)

Figure 2.   Sample of unhealthy retinal images. (a) Abnormal disc/cup ratio, (b) Presence of exudates, (c) Tortuous vessel.

The specifications of the types and conditions of diabetic retinopathy are identified and defined into rules. These rules are built into the algorithm to detect the normal healthy features of the ocular fundus and common symptoms of diabetic retinopathy.

In order to determine whether a retinal image is normal or not, we employ image processing techniques to extract the features of the fundus. The extraction of optic disc seems relatively simple, as the disc is usually the brightest region on retinal images. However, we find that simple edge detection and thresholding image processing techniques do not yield the expected results. Figure 3 shows that the optic disc is inaccurately detected due to the presence of comparatively bright regions near the optic disc.
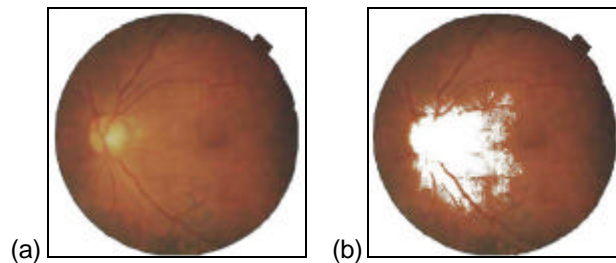

(a)   (b)

Figure 3.   Detecting optic disc using simple thresholding techniques. (a) Original image, (b) Inaccurately detected optic disc.

4　**Preparing the Data**

A whole range of different image processing techniques is used to detect the main fe atures of retinal images as well as the clinical symptoms that indicate the presence of diabetic retinopathy. The following subsections describe each of them in detail.
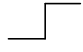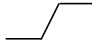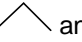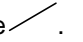
4.1　**Optic Disc and Cup Detection**

The optic disc is the region on the fundus where optic nerves and blood vessel emerge. It appears relatively brighter than the rest of the choroid due to the absence of retina layer. It ranges from round to oval in shape and has an average diameter size of 1.5 to 1.7mm. The optic cup is situated near the centre of the disc and is more pronounced on the temporal half as opposed to the nasal half. The optic cup appears brighter than the optic disc and usually covers less than 40% of the optic disc, although its position, shape and size may vary.

In our approach we employ a combination of the various image processing techniques to accurately detect the optic disc and cup. These include: Sobel edge extraction, varying ellipse fitting, neighbourhood accumulation, and histogram thresholding.

I. Sobel Edge Extraction

An edge is the boundary between two regions of different constant intensity (or grey level). An edge detector looks for regions in an image where the grey levels are changing too quickly to be a random effect, and some look for changes in a specific direction. Basically, locating an edge involves detecting points that fall on the edges. However, the edge points detected at this stage are discrete points and they do not directly show up as an edge. Therefore, a special algorithm is necessary to group all the similar edge points into boundaries. In recent years, many edge point detection algorithms (Davis 1975) have been developed. The most common edge detection method is to analyse the change of intensity gradient where an edge point is said to be present when the magnitude of the gradient exceeds a pre-defined threshold.

Sobel is one of the most well known edge detectors in sensing gradient variation in an image because of their low computation costs and easy implementation, as pointed out by Pitas (1993). Figure 4 shows the convolution masks of the edge detector. *Convolution* is accomplished by a simple multiplication, followed by an addition, and then finally a shifting operation. Sobel edge detector is efficient for different types of edges,

including the "sudden step" edge ⌐, the "slanted step" edge ⟋ , the "roof" edge ⟍ and the "planar" edge ⟋ .

-1	0	1
-2	0	2
-1	0	1

x

1	2	1
0	0	0
-1	-2	-1

y

Figure 4. Sobel edge detector mask of 3×3.

The principal approach of the Sobel operator, $G(x, y)$ is to compute the magnitude of the gradient at each pixel location using the relation,

$$G(x,y)=\sqrt{G_x^2+G_y^2}$$ (1)

where G_x and G_y are the first-derivative operators at any point (x, y) which are defined as

$$G_x=[f(x+1,y-1)+2f(x+1,y)+f(x+1,y+1)]$$
$$-[f(x-1,y-1)+2f(x-1,y)+f(x-1,y+1)]$$ (2)

and,

$$G_y=[f(x+1,y-1)+2f(x,y+1)+f(x+1,y+1)]$$
$$-[f(x-1,y-1)+2f(x,y-1)+f(x-1,y+1)]$$ (3)

where f is the mask value.

In Figure 4, the left mask represents the column gradient while the right mask represents that of the row gradient of the Sobel filter. Sobel filter combines both the row and column gradients to create two orthogonal directions in an image. The mask values of Sobel operator enable it to be more sensitive to both the horizontal and vertical edges.

In our system, the colour retinal image is converted to grey level image before using the simple and fast Sobel edge filter to extract the edges. This filtering operation produces a binary image where the positive (black) data represents edges and the negative (white) data represents uniform texture. The edges detected could be the outline of the optic disc, blood vessel, macular, or any abnormal lesion in the retinal.
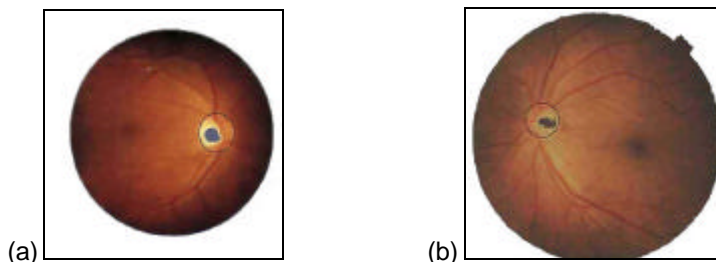
II. Ellipse Fitting

Since the shape of a normal optic disc varies from round to oval, it makes sense to generate a range of ellipses and try to fit them to the edges extracted as described above. The ellipse that has the highest fit is considered to be the optic disc outline. However, we observe that the top and bottom regions of a normal retinal disc rim usually contain main blood crossings from which blood supply is transported to the retina. Therefore it would not be easy for the ellipse fitting function to obtain a perfect fit to the extracted optic disc outline. Hence, some percentage of minimum fit would have to be imposed so that the badly fitted ellipse would not be passed off as the detected optic disc. The numerical figure of the minimum fit is described next.

III. Neighbourhood Accumulation

The fitting of the ellipse is done by running the generated ellipse over extracted optic disc outline and accumulating the pixel values along the way when the ellipses' outline coincide with optic disc outline. To increase the accuracy of the fitting, the accumulation of edge pixel (those pixels that coincide with the ellipses' outline pixels) points includes the neighbouring pixels around the edge pixel. Varying the horizontal and vertical radii of the ellipse generates a range of different sizes of the fitting ellipse. The ellipse that returns the maximum response of accumulated pixel points is regarded as the boundary of the detected optic disc. If the maximum response of accumulated pixel points is lower than the minimum fit then the algorithm have failed to find a normal optic disc; such retinal images would be classified as abnormal.

The minimum fit figure is arrived at by averaging over all the maximum accumulated pixel points of each positively and negatively detected optic disc from a specially chosen set of 20 test retinal images. This set of test images are chosen to give a good measure of the average good fit and bad fit of the ellipse to the extracted optic disc outline.

The range of horizontal and vertical radii of the ellipse is selected so that it is greater than the average normal size of the optic cup to prevent falsely detecting the optic cup as that of the optic disc. Figure 5 shows samples of the optic discs detected.
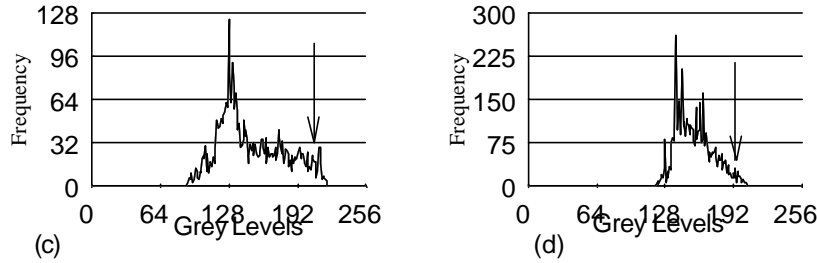

(a)   (b)

(c)

Frequency

128
96
64
32
0

0   64   128   192   256
Grey Levels

(d)

Frequency

300
225
150
75
0

0   64   128   192   256
Grey Levels

Figure 5.   Detection of optic disc and cup. (a), (b) Sample of extracted optic disc and cup . (c), (d) Histograms of the corresponding optic disc showing the threshold grey level (arrow) where the optic cup is segmented from the optic disc.

IV. Histogram Thresholding

The optic cup is defined to be the brightest region within the optic disc. In the detection of the optic cup, a survey of the histogram distribution of the optic disc region reveals an interesting pattern. When a threshold is set at the second highest 'peak' of grey levels in the histogram with respect to the maximum grey level (walking from the right side of the histogram of 256), a reliable and accurate optic cup region is extracted.

Thresholding is used in image processing to separate an object's pixels from the background pixels. This technique converts a multi-grey level image into a binary image containing only two distinct grey levels. The threshold operation may be defined as

$$g(x, y) = \begin{cases} G_O & if \quad f(x, y) > T \\ G_b & if \quad f(x, y) \le T \end{cases} \tag{4}$$

where $f(x, y)$ is the original image, $g(x, y)$ is the threshold-processed image, T is the threshold value, G_O is the object grey level value after thresholding operation, and G_b is the background grey level value after the thresholding operation. The objects in an image can be separated effectively from a background by grouping the pixels that share common grey levels.

Figure 6.   Principle of thresholding a grey level histogram.
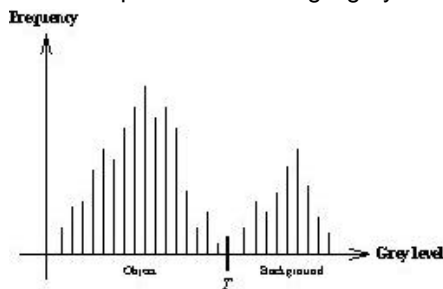
In Figure 6, a dark object in an image $f(x, y)$ can be extracted from a light background by choosing a suitable threshold T (a particular intensity level) between the two grey regions.   Then, any point (x, y) in the image that has a grey level lower than the value of T is considered an object point; otherwise, the point is called a background point.   In other words, the objective is to generate a binary image $g(x, y)$ containing only the object points as defined in (4). The ratio of the optic cup to disc is calculated as the pixel area of the detected optic cu p to the corresponding area of the detected optic disc.

4.2   Exudates Detection

The presence of exudates indicates retinal disorders and is associated with patches of vascular damage. Exudates usually show up as white patches (in grey images; yellowish in colour images) of varying sizes and shapes scattered randomly in vascular spaces. Simple thresholding techniques do not give a satisfactory result as some smaller exudates have about the same intensity as the background of the retinal. Hence, we used a more effective method that employs the minimum distance discriminant (Kressel U and Schurmann, 1997; Castleman, 1996) to detect the exudates.

4.2.1 Minimum Distance Discriminant

Each pixel in colour digital image consists of three basic spectrum features (or colour features) in red, green and blue planes and each plane has its own illuminance. In general, different types of objects in digital images have their own range of spectrum features so that they appear in various colours and form different clusters (or classes) based on their spectrum features in the RGB colour space. In general, the greater the spectrum

distance between the centres of different classes, the easier it is to identify the boundaries of different objects that belong to different clusters.

Utilising Bayes' theorem (Bayes, 1763) we can reliably carry out the classification of different objects belonging to each class. Bayes' theorem states the rule for updating belief H given state of evidence E, and background knowledge (context) I:

$$p(H|E,I) = p(H|I)* p(E|H,I) / p(E|I) \tag{5}$$

The term $p(H|E,I)$ is called the posterior probability, and it gives the probability of H after considering the effect of evidence E in context I. The $p(H|I)$ term is just the prior probability of H given I alone; that is, the belief in H without the evidence E being considered. The term $p(E|H,I)$ is called the likelihood, and it gives the probability of the evidence assuming H and background knowledge I is true. The last term, $1/p(E|I)$, is independent of H, and can be regarded as a normalising or scaling constant. The information I is a conjunction of all of the other statements relevant to determining $p(H|I)$ and $p(E|I)$.

Let $\mathbf{C}_i(c_r, c_g, c_b)$ be the mean value vector of spectrum feature of class i in RGB space, where i=1,2,…N and N is a class number in an image. Let $\mathbf{X}(x_r, x_g, x_b)$ be the measurement vector of pixel X, that is, X's illuminance in RGB space. Let $F_i(\mathbf{X})$ be the discriminant function for classifying pixel X into class i.

Let $p(\mathbf{C}_i/\mathbf{X})$ be the conditional probability (posterior probability). It represents the probability of $\mathbf{X}$ belonging to class i using the particular pixel's spectrum feature vector $\mathbf{X}(x_r, x_g, x_b)$. If it is found that $p(\mathbf{C}_i/\mathbf{X}) > p(\mathbf{C}_j/\mathbf{X})$, where j=1,2,…N and j≠i, then it can be concluded that $\mathbf{X}$ belongs to class i.

According to Bayes' theory, $p(\mathbf{C}_i/\mathbf{X})$ can be expressed as:

$$p(\mathbf{C}_i/\mathbf{X}) = p(\mathbf{C}_i) * p(\mathbf{X}/\mathbf{C}_i) / p(\mathbf{X}) \tag{6}$$

Where $p(\mathbf{C}_i)$ is the priori probability of class i in the image to be classified. $p(\mathbf{X}/\mathbf{C}_i)$ indicates the class specific probability distribution of $\mathbf{X}$.

In (6), $p(\mathbf{X})$ is independent of class i so it can be safely discarded here. So the discriminant factor can be defined as,

$$F_i(\mathbf{X}) = p(\mathbf{C}_i) * p(\mathbf{X}/\mathbf{C}_i) \tag{7}$$

Here it is reasonable to assume $p(\mathbf{X}/\mathbf{C}_i)$ is a normal distribution,

$$p(X/C_i) = \frac{1}{\sigma^{1/2}\sqrt{2\pi}} \exp\left(-\frac{(X-C_i)^T}{2\sigma}\right) \tag{8}$$

Where σ is the covariance and is defined as

$$\sigma = \sum_i^N (X - C_i) \tag{9}$$

and $p(\mathbf{C}_i)$ is constant for i=1,2,…N.

It can be further assumed that the covariance σ is almost constant for all classes. So the

simplified discriminant $F_i(\mathbf{X})$ is redefined as

$$F_i(X) = X^T X - 2C_i^T X + C_i^T C_i \tag{10}$$

where X^T and C_i^T refer to the matrix component of illuminance X and feature spectrum C_i of class i, respectively. Finally the concept of "minimum distance" is used to replace the maximum discriminant $F_i(\mathbf{X})$,

$$D_i(X, C_i)^2 = -F_i(X) = 2C_i^T X - X^T X - C_i^T C_i \tag{11}$$

The minimum distance discriminant from (11) is the classification function that is used to detect exudates in retinal images.

4.2.2 Extraction of Exudates

We observe that a colour retinal image consists of two main classes, yellowish patches (exudate) and reddish vessel and background. The spectrum feature centre, C_{exdt} and C_{bkgmd} of the two classes can be easily obtained by selecting a small window in the exudates region and the background region respectively in the training samples. The training samples are specially chosen from a set of retinal images that contain exudates. Then the mean illuminance of the two windows can be tabulated and stored as prior information as $C_{exdt}(C_r, C_g, C_b)$ (ie. C_{exdt}) and $C_{bkgmd}(C_r, C_g, C_b)$ (ie. C_{bkgmd}), respectively.

During the processing of retinal images, for each pixel $X(x_r, x_g, x_b)$, the distance $D(X, C_i)$ from itself to class center C_i (C_{exdt} and C_{bkgmd}) is calculated. If $D_{exdt}(X, C_{exdt})$ is smaller than $D_{bkgmd}(X, C_{bkgmd})$, then the pixel X is classified as exudates otherwise it is being classified as background pixel. Figure 7 shows a sample of detected exudate.
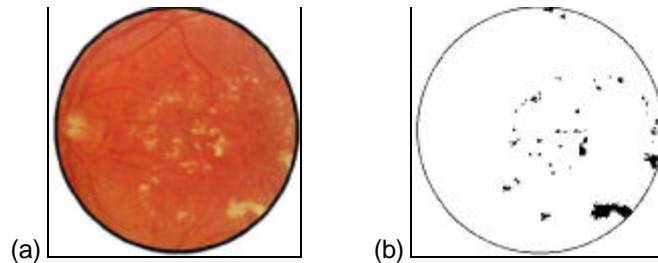
Figure 7.   Detection of exudate. (a) Original image, (b) Detected exudate.

4.3   Vessel Detection

The cross section profile of the retinal blood vessel resembles a 'ridge' with the points running through the centre of the vessel having the highest intensity and these intensity levels tend to taper off toward the boundaries of the vessel. Figure 8 shows the cross section profile of a typical retinal blood vessel. Chaudhuri *et al.* (1989) used a two-dimensional matched filter, approximated by Gaussian fitting function to detect the retinal blood vessels. *Gaussian kernel* is a popular filter used for smoothing or fitting function as it models after 'bell' shape characteristics. Our approach to detect retinal vessel is adapted from this method.
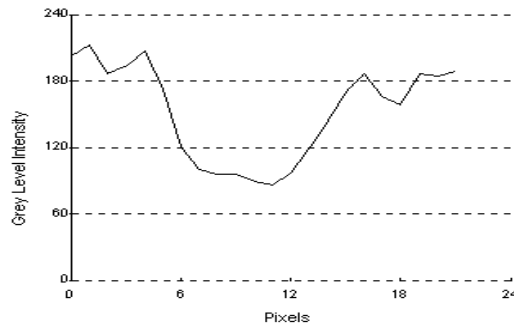

Figure 8.   Cross section profile of a typical retinal blood vessel.

We investigated the properties of retinal blood vessels to develop image processing algorithms to detect the outlines of the vessels precisely. The main properties observed are:

If the vessel is divided into segments along its length, then the segment direction will vary continuously. The change of direction between segments is a smooth continuous function.

The width of the segment varies continuously. There is no abrupt step change in the width of the vessel segments and there is always a smooth transition between adjacent segments.

The density distribution of a blood vessel cross sectional profile can be estimated using Gaussian shaped function. The density distribution is smooth and never exhibits any step-like appearance.

Our vessel detection algorithm is as follows:

I. Smoothing

The input grey image is smoothed by a 5×5 mean filter to reduce the spurious noise effects. Low pass spatial filters are used to smooth high spatial frequencies and accentuate low spatial variations in an image. These filters are characterised by positive values in their masks, which clearly yields an additive, hence smoothing effect between neighbourhood pixels during the convolution process. The overall effect is to smooth noisy edges and they are also known as *smoothing filters*. Neighbourhood can be achieved using the relation,

$$q(x,y) = \frac{1}{N} \sum_S p(x,y) \qquad (12)$$

where $p(x,y)$ and $q(x,y)$ are the original and smoothed images respectively, S is a set of co-ordinates of points in the neighbourhood of (x,y), and N is the total number of pixels in the neighbourhood. Each pixel is replaced with the average of itself and its neighbours.

II. Matched-filter Convolution

The smoothed-image is convolved with a set of two-dimensional matched filters. The two-dimensional matched filters are approximated with the Gaussian fitting function, as its profile matches the cross-sectional profile of a typical vessel. The filters consist of twelve different kernels, with each kernel specifically rotated to optimise for a different vessel angular direction. The angular difference between each kernel is chosen to be 15°. Hence, a total of twelve kernels are needed to accommodate the 180° of possible vessel directions. Each kernel is a set of 15×15 matrix-floating points. Each pixel of the smoothed-image is convolved with the twelve filters and only the maximum response of each convolution is retained.

III. Histogram Thresholding

The matched-image is then converted into a histogram and an automatic thresholding algorithm, where the threshold is selected to be the highest few percentage of response, is applied to retrieve the enhanced vessels from the background.

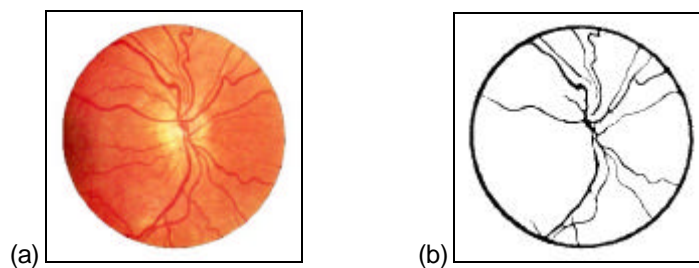Figure 9 shows an example of the original retinal image and extracted vessel.

(a)   (b)

Figure 9.   Detection of retinal vessel. (a) Original image, (b) Extracted vessel.

4.3.1 Vessel Tortuosity Detection

One of the symptoms of diabetic retinopathy is the presence of new vessel formation, often appears as tortuous vessel. Hence, the detection of tortuous vessel is important in the screening of diabetic retinopathy. In our system, a skeletonisation algorithm is used to extract the centre line of the vessel points. The resulting output contains only the centre line pixels outlining the extracted blood vessel, as shown in Figure 10. The *Skeletonisation* operation involves thinning an image to remove extra redundant pixels until it produces a simpler image. The characteristics of a skeletoned image are: (i) it should consists of thin regions of one pixel wide; (ii) the pixels that make up the skeleton should lie near the centre of a cross section of the region; and (iii) the skeletonisd pixels must be connected to each other to form the same number of regions as in the original image.
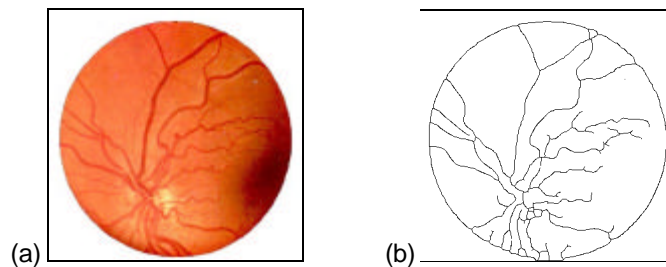
(a)   (b)

Figure 10.   (a) Original image with tortuous vessel. (b) Centre line
               pixel outline of the extracted vessel of (a).

The detection of tortuous vessel is carried out by walking along the centre line of the extracted vessel and tabulating the curvature of the outline. Curvature can be defined in a number of ways which we will describe in the following subsections.

4.3.2 Absolute Direction Change

When tracking a centre line of a chosen segment of the blood vessel, each direction change along the path can be accumulated. At the end of the tracking, the number of direction changes indicates how tortuous is the segment. The direction change, hereby refer to as *DirChg*, of each pixel of the centre line is calculated by drawing an imaginary line from the fifth pixel point prior to the current pixel to the fifth pixel point ahead. The direction of this imaginary line is differentiated with the imaginary line collected from the previous pixel point. This differentiation value determines that there is a *DirChg* if the angle difference between the two imaginary lines is greater than a fixed angle, in this case it is chosen as $30°$. The integration of all the *DirChg* of all the pixel points along the centre line of the segment of blood vessel gives a measure of tortuosity of this segment of the vessel. However, this *DirChg* only gives an indication of a measure of curvature at localised regions along the segment and it does not give an indication of how straight the segment is just before or after the *DirChg*. It can be seen in Figure 11 that both segments of the vessel contain almost the same curvature of *DirChg.* However, if the range of pixel points near the *DirChg* pixels is taken into account, then the segment of vessel in Figure 11b can be observed to be more tortuous than that in Figure 11a. This is due to the fact that the vessel in Figure 11a has a gradual curve while that of Figure 11b has a more abrupt curve.
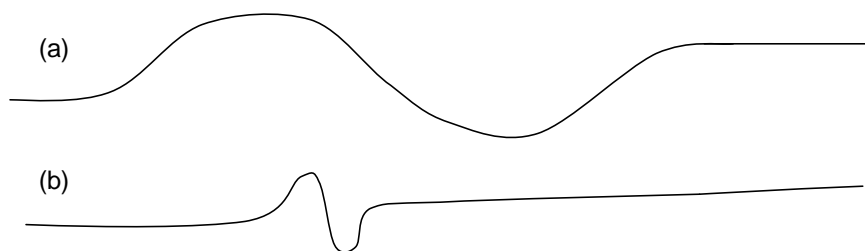
(a)

(b)

Figure 11.   Curvature as a measure of *DirChg*. (a) Gradual change of
             direction. (b) Localised abrupt change of direction.

4.3.3 Arc to Chord Ratio

Another definition of curvature is the simple arc to chord ratio, hereby known as *ACurve*. If a segment of the vessel is chosen which contains some degree of curvature, then this curvature can be calculated by taking the arc length and dividing it by its chord length, as shown in Figure 12. The arc length is the length of the blood vessel while the chord length is the Euclidean distance between the start and end point of the blood vessel. The greater the ratio is, the higher is the curvature or tortuosity of the blood vessel. The arc to chord ratio can be normalised with respect to the arc length and the chord length to give an average value over the length of the vessel, known as *ACURVEarc* and *ACURVEchord* respectively. However, this measure of tortuosity is accurate only if the start and end point of the segment of vessel contains a single arc. This measure of tortuosity of a segment of a blood vessel only indicates whether a segment contains any curves and would not indicate what degree of curvature the segment holds (Figure 12b).
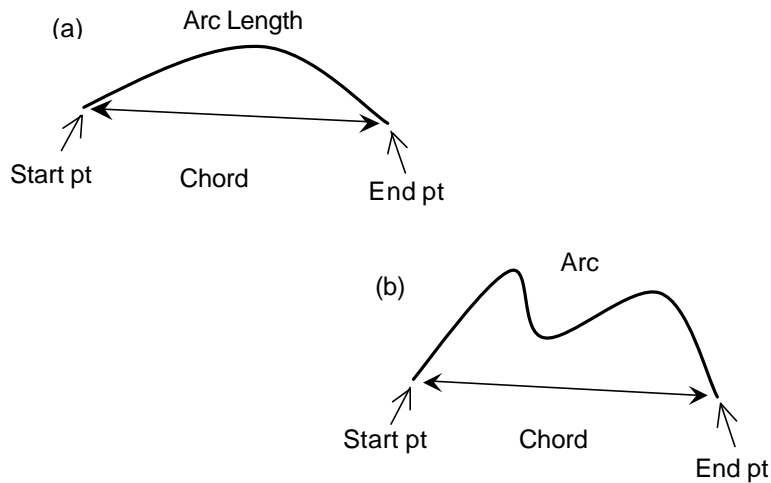
Figure 12.   Curvature as a measure of arc to chord ratio. (a) Start and end point containing single arc. (b) Start and end point containing multiple arcs.

4.3.4 Curvature Based on Paths

Mokhtarian and Mackworth (Mokhtarian and Mackworth, 1986) introduce the curvature of a particular point on a line with respect to its x and y components as,

$$k(t) = \frac{x_0(t)\, y_1(t) - x_1(t)\, y_0(t)}{\left(x_0(t)^2 + y_1(t)^2\right)^{\frac{3}{2}}} \tag{13}$$

where $k(t)$ is the curvature measure at point t, $(x_0(t),\, y_0(t))$ is the pixel co-ordinates at point t, $(x_1(t),\, y_1(t))$ is the co-ordinates chosen to be five pixels ahead of point t $k(t)$ is hereby referred to as *kCurve*. The normalised version of *kCurve* is *kCurvearc* and *kCurvechord*, where the former is normalised with respect to the total segment's arc length and the latter is normalised with respect to the total segment's chord length.

4.3.5 Curvature Based on Line Fitting

Anderson *et al.* (1984) and O'Gormann (1988) propose an alternate definition of curvature estimation of a particular point on a line which is based on the angular difference between two straight lines fitted to the curve at some fixed pixels apart. Then the curvature point *t* can be defined as,

$$K(t) = \frac{da}{ds}(t) \tag{14}$$

where $K(t)$ is the curvature measure at point t, a is the difference of the angle of the two tangent lines at point t, s is the arc length between the tangent line at point t and the other tangent line, which is chosen to be five pixel ahead of point t. $K(t)$ is hereby referred to as *aCurve*. The normalised version of *aCurve* is *aCurvearc* and *aCurvechord*, where the former is normalised with respect to the total segment's arc length and the latter is normalised with respect to the total segment's chord length.

5. Data Mining

The above definitions of curvature do not individually give a reliable and consistent indication of the overall measure of tortuosity of the vessel segment under consideration. However, we observe that if some of the attributes of the different curvature definitions are used collectively, then

the degree of reliability and accuracy in measuring the curvature of a particular segment of the retinal vessel is increased. In ADRIS, we combine all the data of the 12 attributes associated with the four curvature definitions and feed the data into an association based data mining classification tool, CBA. The output of CBA consists of a set of association rules governing the relationship between the 12 attributes that reliably and accurately classify the input vessel segment.

The rules generated by CBA are incorporated into the vessel tortuosity detection algorithm. Each of the rules generated indicates the association between the tortuosity measure given by each curvature definition. Collectively, when these rules are applied to each unseen segment of the vessel under consideration, the algorithm would classify whether the vessel is tortuous or otherwise.

6   Evaluation of the Discovered Knowledge

In Singapore, all diabetic patients are required to undergo an annual eye screening in Government-run medical clinic. We obtained a total of 310 retinal photographs from this screening exercise and digitised them to generate the retinal images. These images are used in our experiments to detect the optic disc and cup, and exudate. In addition, more than 1000 vessels are automatically extracted for the vessel detection experiment.

There are two types of retinal images, normal and abnormal. Normal retinal images shows healthy retina. Abnormal retinal images contains symptoms of diabetic retinopathy or age-related disease such as cataracts and glaucoma where the former causes the retinal image to appear hazy or opaque, and the latter exhibits high optic cup to disc ratio.

There are three main phases in the development of the ADRIS: (1) image preparation, (2) image processing and (3) review. The first phase includes digitising the retinal photos and pre-processing them. The second phase consists of processing those images which involve medical expert input to specify the features that discriminate normal and abnormal retinal images. Any abnormal retinal images are presented to the doctor for review in the last phase. We discuss each of these phases in detail:

I. Image Preparation

The inputs to the system consist of a pair of digital fundus images obtained from a colour fundus camera for each patient. The images are converted from high-resolution Polaroid colour photographs to digital format through an image scanner device. These digital images are expected to exhibit a relatively distinct outline of the main features of a healthy retina, namely the optic disc, optic cup, main blood vessels and macular. For unhealthy retina, symptoms of the corresponding eye diseases must be clearly visible and distinctly detectable with human vision. The resolution of the digital images are scanned with a minimum of 1k $\times$ 1k $\times$ 24 bits.

This phase is also known as the pre-processing phase where the images are digitally prepared prior to feeding them to the next processing phase. Pre-processing operations include removal of noise and artefacts (introduced during digitising process) with smoothing filter, and re-sizing the digital image to a standard size of 400$\times$400$\times$24bits.

II. Image Processing

Retinal digital images are first filtered through the specifications of *Normal* (healthy) retina. The initial phase detects the optic disc and cup, followed by the presence of main blood vessel of a minimum total length and average width. The next phase detects symptoms of diabetic eye diseases which includes abnormal optic cup to disc ratio and the presence of exudates and tortuous vessels. The choroid intervascular region should contain only uniform background and should not contain any patches of variation.

III. Review

This last phase classifies the retinal images into *Normal* and *Abnormal* cases. Input images with healthy fundus features and with no detected abnormal conditions are classified as *Normal*. Otherwise, the images are classified as *Abnormal*. Abnormal images are highlighted for the doctor's attention.

6.1   Optic Disc and Cup Detection

Out of 310 retinal images used for this experiment, 252 images has visible and normal optic disc to cup ratio, 58 images has poor visibility and/or blur optic disc outline, 75 images has poor visibility of optic cup and/or incorrect optic cup to disc ratio. The experimental results of optic disc and cup detection are discussed separately in the following two subsections.

6.2 Optic Disc Detection

The optic disc processing algorithm is able to correctly classify 227 images with disease free optic disc as *Normal* (true-positives), 25 images with disease free optic disc as *Abnormal* (false-positive) and all the 58 images with symptoms of irregular optic disc as *Abnormal* (true-negatives). In other words, the detection performance is 90.1% for true-positive, 9.9% of false-positive, and 100% of true-negative. An image is considered to be true-positive when the automatically detected optic disc outline is visually compared with the visually detected ellipse outline and the difference between the two centres of the ellipses is found to be less than 5 pixels apart. That means with an image resolution of 400$\times$400 pixels, the maximum error rate is 6.25% (100%*5*5/400). Figure 13 shows examples of false-positive and true-negative detections. 25 images with normal optic disc are detected as abnormal because of poorly defined outline of optic disc.
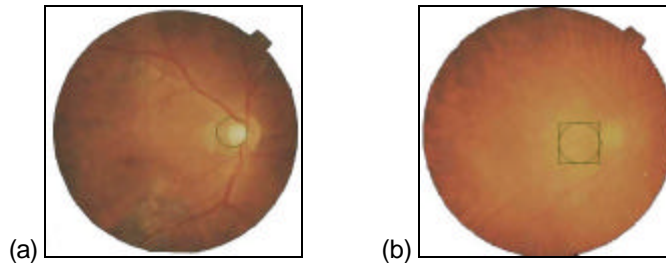

(a)   (b)

Figure 13. Detection of optic disc. (a) False-positive due to ill-defined optic disc outline (circle registers falsely detected optic disc), (b) True-negative (square-enclosed-circle represents the approximate disc area which the algorithm identified as abnormal optic disc due to normal disc area not found $\rightarrow$ disc area larger than normal).

6.3 Optic Cup Detection

The optic cup processing algorithm correctly classifies 204 images with disease free optic disc as *Normal*, 31 images with disease free optic cup as *Abnormal* (false-positive) and 75 images with symptoms of irregular optic cup to disc ratio as *Abnormal* (true-negative). In other words, the success rate is 86.8% of true-positive, 13.2% of false-positive, and 100% of true-negative. Part of the reason that there are 31 images being wrongly classified as false-positives is due to incorrect detected optic disc, as shown in Figure 14. The other reason for false-positives is the poor contrast brightness of the optic cup and disc, inherent in the retinal

photographs. The optic cup is considered to be correctly detected by comparing the automatically extracted cup with the manually extracted one.
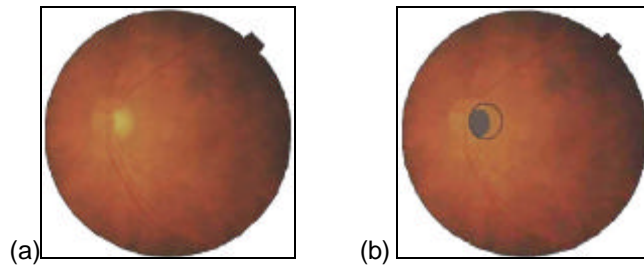

Figure 14.   False-positive detection of optic cup. (a) Original image. (b) The wrongly detected optic cup (black region within the circle) where it's location is not in the middle of the inaccurately detected disc (circle).

6.4   Exudates Detection

A total of 23 images with visible exudates are identified by medical expert. ADRIS is able to correctly classify 23 of the images that contain exudates as *Abnormal* (100% true-negatives), 75 images with no presence of exudates as *Abnormal* (26.1% of false-negatives) and the remaining 212 with exudate free images as *Normal* (73.9% true-positives). There are 75 images that do not contain any symptoms of exudates but are incorrectly classified as having exudates. These errors are due to the presence of relatively bright patches of variation scattered around the choroid regions and as a result, the algorithm incorrectly identified them as having the same spectrum features as that of exudate. These relatively bright patches of variation are mainly due to artefacts introduced during the fundus photography or digitisation process. Figure 15 shows an example of incorrectly detected images (false-negatives).
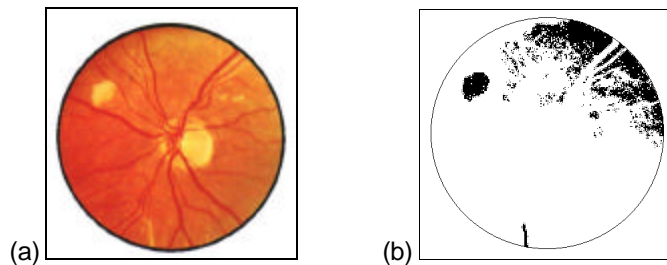
Figure 15.   Errors in exudate detection. (a) Original image. (b) False-positive reflected on the upper right region (black pixels) due to the its relative brightness (same spectrum features as the exudates).

6.5   Vessel Processing

The processing of retinal vessels consists of two stages. First, the main vessels, those with average width greater than 90µm (5 pixels) and average length greater than 30 pixels (540µm) are extracted. Second, these extracted vessels are processed into single pixel width of connected lines from which the tortuosity of the vessel is measured.

Each of the main vessels is automatically extracted from the retinal images. On average about 4 vessel segments are successfully extracted from each image and they are visually verified. In Figure 16, an example of tortuous vessel is highlighted.
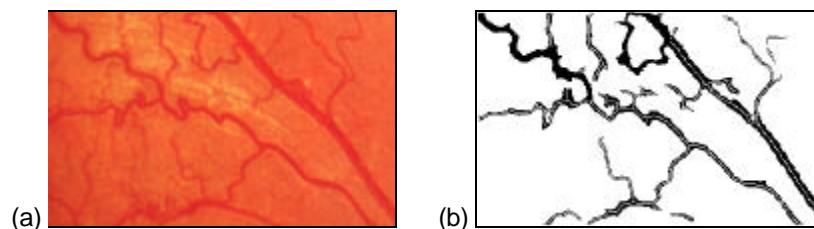

(a)   (b)

Figure 16.   Detection of tortuous vessel. (a) Original image, (b) Some of the detected tortuous vessel (darken portions)

Out of the total 310 images, 35 of them contain almost featureless image, possibly caused by cataracts. A total of 1205 main vessel segments are automatically extracted. The vessel tortuosity detection algorithm extracted 12 attributes (Sections 3.4.1 to 3.4.4) from each vessel segment and fed them into the CBA classification tool. We configure CBA to mine at 35% minimum support[1], 50% minimum confidence[2], 30% of data used as

---

[1]   Minimum support refers to a constraint in classification technique whereby it gives a minimum percentage of the number of transactions in the data set that supports a rule.

[2]   Minimum confidence is a constraint that gives the minimum percentage of confidence that the number of transactions in the data set satisfy both the left-hand-side and right-hand-side items in an association rule. For example in an association rule, $X \Rightarrow Y \mid C$ implies that X (a set of items in data set T) is associated to Y (a single item in T and which is not present in X) has a confidence that C% of transactions in T that satisfy X also satisfy Y.

training cases and 10 times cross validation[33]. CBA generated 11 association rules with a cross-validation error rate of 12.1%.

7 Using the Discovered Knowledge

We used these association rules to determine whether a vessel is normal or tortuous. If a retinal image contains at least one tortuous vessel, then it will be classified as abnormal. In total, the rules detected 95 vessels as tortuous.

8 Conclusion

In this paper, we have shown that images captured from Diabetic Retinopathy Screenings can be fed into a computer system for automatic classification. ADRIS can detect symptoms such as the size of optic disc and cup, and its ratio; exudates or unspecific lesion in the intervascular region; and the presence of tortuous main vessel. Experimental results show that the basic features of the retina and diabetic retinal disease can be detected.

The performance of the optic disc and cup detection algorithm as well as its ratio calculation is found to be up to expectation, as verified by the various doctors working with us on this system. Likewise the detection of the exudate and the detection of tortuous vessel is within expectation. We also found out that a large proportion (74%) of the retinal images obtained from the screening exercise is normal, where only 80 retinal images are abnormal out of the total 310 images.

---

[3] Cross-validation is a way to test how accurate is the classification. It is done through executing the system over a number of folds (or times) over the data which is being split into training case and testing case. The output of cross validation gives the average error rate accumulated after applying the classification rules on the unseen test data.

Most importantly, the occurrence of false-negatives, where the presence of abnormal features fails to be detected by the system does not happen in ADRIS.

Our future works include identifying more advanced diabetic retinopathy symptoms with an ophthalmologist's input.

Acknowledgement

Reference

Lim KH, 'Registration of New Blindness in Singapore for 1985-1995', *Singapore Medical Journal*, vol. 40, no. 2, Feb 1999.

Goh LG, 'A Diabetes Centre In The Community', *Singapore Medical Journal*, vol. 30, no. 3, Mar 1998.

Kahn HA, Hiller R, 'Blindness caused by diabetic retinopathy', *Am. J. Ophthal*., vol. 78, pp. 58-67, 1974.

Palmberg PF, 'Diabetic Retinopathy', *Diabetes*, vol. 26, pp.703-709, 1977.

Klein R, Klein Bek, Moss SE, Cruickshanks KJ, 'The Wiscousin Epidemiologic study of diabetic retinopathy. XV. The long term incidence of macular edema', *Ophthal*., vol. 102, pp.7-16, 1995.

Javitt JC, Canner JK, Sommer A, 'Cost effectiveness of current approaches to the control of retinopathy in type I diabetics', *Opthal*., vol. 96, pp.255-264, 1989.

Ghafour IS, Allan D, Foulds WS, 'Common causes and blindness and visual handicap in the west of Scotland', *Brit. J. Ophthal*, vol. 67, pp.209, 1983.

Singer DE, Nathan DM, Fogel HA, Schachar AP, 'Screening for diabetic retinopathy', *Ann. Intern. Med*, No. 116,, pp.660-671, 1992.

Retinopathy Working Party, 'A protocol for screening for diabetic retinopathy in Europe', *Diabetic Med*., no. 8, pp.263-270, 1991.

Gardner GG, Keating D, Willaimson TH, Elliot AT, 'Automatic detection of diabetic retinopathy using an artificial neural network:a screening tool', *Brit. J. Ophthal*., vol. 80, pp. 940-944, 1996.

Ward NP, Tomlinson S, Taylor CJ, 'Image analysis of fundus photographs. The detection and measurements of exudate associated with diabetic retinopathy', *Ophthal.*, vol. 96, pp. 80-86, 1989.

Spencer T, Phillips RP, Sharpe PF, Forrester JV, 'Automatic detection and quantification of microaneurysm in fluoresceins angiograms', *Graefe's Arch. Clin. Exp. Ophthal*, vol. 230, pp 36-41, 1992.

Spencer T, Phillips RP, Sharpe PF, Ross T, Forrester JV, 'Quantification of diabetic maculopathy by digital imaging of the fundus', *Eye.*, vol. 5, pp 130-137, 1991.

Katz N, Goldbaum M, Nelson M, Chaudhuri S, 'An image processing system for automatic retina diagnosis', *SPIE*, vol. 902, pp. 131-7, 1988.

Katz N, Goldbaum M, Nelson M, Hart LR, 'The discrimination of similarly colored objects in computer images of ocular fundus', *Invest. Ophthal. Vis Sci.*, vol.31, pp. 617-627, 1990.

Cox MJ, Wood CJ, 'Computer-Assisted optic nerve head assessment', *Ophthal. Phy. Opt.*, vol. 11, pp. 27-35 , 1991.

Morris T, Wood I, 'On the Automatic Identification of the Optic Nerve Head', American Academy of Optometrists Biennial Meeting in Europe, Presentation, 1994.

Phillips RP, Sharpe PF, Forrester JV, 'Automatic detection and quantification of retinal exudate', *Graefe's Arch. Clin. Exp. Ophthal*, vol. 231, pp 90-94, 1993.

Leistritz L, Schweitzer D, 'Automated detection and quantification of exudate in retinal images', *SPIE: Appl. Digital Image Proc. XVII*, vol. 2298, San Deigo, July 94.

Zhou M, Rzeszotarski S, Singerman LJ, Chokreff JM, 'Detection and quantification of retinopathy using digital Angiogram', *IEEE Trans. Medical Imaging*, vol. 13, no. 4, pp. 619-626, 1994.

Zana F, Klein JC, 'Robust segmentation of vessels from retinal angiogram', *Proc. DSP*, pp. 1087-1090, 1997.

Capowski JJ, Kylstra JA, Freedman SF, 'A numeric index based on spatial-frequency for the tortuousity of the superficial femoral artery in early atherosclerosis, *J. Vasc. Res.*, vol. 30, pp. 181-190, 1993.

Elomaa T, Holsti N, 'An experimental comparsison of inducing decision tress and decision lists in noisy domain', *Proc. 4th Europ. Work. Session on Learning*, Montpeiller, pp. 56-69, Dec 1989.

Lesmo L, Saitta L, Torasso P, 'Learning of fuzzy production rules for medical diagnosis', In Gupta MM, Sanchez E(eds*.), Approx. Reasoning in Decision Analysis*, North Holland, 1982.

Brako I, Kononenko I, 'Learning Rules from incomplete and noisy data', in B Phelps(eds.), *Interaction in AI and Stat. Methods*, Hampshire: technical press, 1987.

Hojker S, Kononenko I, Jauk A, Fidler V, Porenta M, 'Expert's system development in the management of thyroid diseases', *Proc. Europ. Congress for Nuclear Med*., Milano, Sept 1988.

Kern J, Dezelic G, Tezak-Bencic M, Durrigl T, 'Medical decision making using inductive learning program', *Proc. 1st Congress Yugos. Med. Info.*, Beograd, pp. 221-228, Dec 1990.

Muggleton S, 'Inductive acquisition of expert knowledge', Turing Institute Press and Addison-Wesley, 1990.

Provan GM, Singh M, 'Datamining and model simplicity: a case study in diagnosis', *Proc. 2nd Int. Conf. KDD.*, pp. 57-62, Oregon, Aug 1996.

Nunez M, 'Decision tree induction using domain knowledge', in Wielinga B et al. (eds.), *Current Trends in Knowledge Acquisition*, IOS Press, 1990.

Liu B, Hsu W, Ma Y, 'Integrating Classification and Association Rule Mining.' *Proc. 4th Int. Conf. KD. and DM* (KDD-98, Plenary Presentation), New York, USA, 1998.

Davis LS, 'SURVEY: A Survey of Edge Detection Techniques,' *Computer Graphics and Image Processing*, vol. 4, pp. 248-270, 1975.

Pitas I, 'Digital Image Processing Algorithms', Prentice Hall, ISBN 0-13-145814-0, 1993.

Kressel U, Schurmann J, 'Pattern dassification techniques based on function approximation', In 'Handbook of character recognition and document image analysis', Bunke H, Wang PSP (eds.), ISBN : 981022270X, *Singapore : World Scientific*, 1997.

Castleman KR, 'Digital image processing', ISBN : 0132114674, Englewood Cliffs, N.J. : Prentice Hall , c1996.

Bayes, Rev. T., "An Essay Toward Solving a Problem in the Doctrine of Chances", Philos. Trans. R. Soc. London 53, pp. 370-418 (1763); reprinted in Biometrika 45, pp. 293-315 (1958), and Two Papers by Bayes, with commentary by W. Edwards Deming, New York, Hafner, 1963.

Chaudhuri S, Chatterjee S, Katz N, Nelson N and Goldbaum M, 'Detection of Blood Vessels in Retinal Images Using Two-Dimensional Matched Filters', *IEEE Transaction on Medical Imaging*, vol. 8, no. 3, Sept 1989.

Mokhtarian F, Mackworth A, 'Scale-based description and recognition of planar curves and two dimensional shapes', *IEEE Trans. Pattern Anal. Mach. Intell.*, vol. 8, pp.34-43, 1986.

Anderson IM, Bezdek JC, 'Curvature and deflection of discrete arcs:A theory based on the commentary of scatter matrix pairs and its application to vertex detection in planar shape data', *IEEE Trans. Pattern Anal. Mach. Intell., vol.*6, pp. 27-40, 1984.

O'Gormann, 'An analysis of feature detectability from curvature estimation', *Proc. IEEE Conf. Comp. Vis. Pattern Reco*., Ann Arbor, M1, pp. 235-240, 1988.

Fayyad U, Piatetsky-Shapiro G, Smyth P, 'Knowledge discovery and data mining:toward a unifying framework', *KDD96*, pp. 82-88, 1996.